Photoassociation and bound-bound excitation into the 2 $^2\Pi$ state of LiZn, LiCd, and NaZn molecules

Davorka Azinović, Xinghua Li,* Slobodan Milošević, and Goran Pichler
Institute of Physics, University of Zagreb, P.O. Box 304, HR-10000 Zagreb, Croatia
(Received 5 July 1995)

The photoassociation and bound-bound excitation processes of alkali-metal–group-II*B* molecules have been studied for the LiZn, LiCd, and NaZn molecules. We considered two main factors relevant to these processes, namely, the densities of collision complexes and the relevant absorption coefficients. Densities in the vapor mixture were manipulated by preparation of different metal alloys, whereas the free-bound or bound-bound absorption is selected by changing a laser wavelength used for the excitation. The 2 $^2\Pi$ states were directly excited by the laser wavelength in the spectral range 435–450 nm. The densities of the LiZn, LiCd, and NaZn excimers were estimated from alkali-metal and Zn (Cd) densities using the dissociation equilibrium equation for the corresponding excimers in the ground state. The experimentally observed LiZn excimer band at 477 nm was satisfactory compared with the appropriate theoretical simulation, assuming free-bound excitation of the 2 $^2\Pi$ state at 438.5 nm.

PACS number(s): 33.20.Kf, 33.80.Gj, 34.50.Ez

I. INTRODUCTION

Photoassociation is an optically assisted collision in which a colliding pair of atoms in the ground state absorbs a photon, resulting in the production of an electronically excited diatomic molecule. Theoretical treatment of the photoassociation process has been presented by Doyle [1] for the calculation of the H_2 $b^3\Sigma_u^+ \rightarrow a^3\Sigma_g^+$ absorption coefficient. Sando and Dalgarno [2] also reported a similar treatment for the He_2 $X^1\Sigma_g^+ \rightarrow A^1\Sigma_u^+$ transition. Other molecules, such as alkali-metal–rare-gas, group I*A*, II*A*, and II*B* diatomic molecules, have also been studied through the photoassociation process [3–6]. Quite recently photoassociation has become a very important tool to study long-range molecules in ultracold atomic collisions [7–9].

Recently we have reported the experimental observations and quantum-mechanical simulations of LiZn [10–13], LiCd [11,12,14], and NaZn [15,16] blue-green $2\,^2\Pi \rightarrow 1\,^2\Sigma^+$ emission produced in a photochemical reaction. These studies show an interplay of the bound-bound and the bound-free emission intensities depending on the vibrational distribution of the upper electronic states. It is shown that the bound-bound transitions play a dominant role for the first few vibrational levels of the 2 $^2\Pi$ state, whereas the bound-free transitions become gradually more important in the overall emission spectrum as vibrational number increases [11,12]. The bound-bound excitation was first experimentally observed in the case of the LiHg excimer [12,17].

The preparation of intermetallic molecules by a photochemical reaction such as

$$\mathrm{Li}_2(2\,^1\Pi_u) + \mathrm{Zn}(4S) \rightarrow \mathrm{LiZn}(2\,^2\Pi) + \mathrm{Li} \qquad (1)$$

has a disadvantage since the nascent rovibrational distribution in the upper state cannot be easily determined. This causes difficulties in testing the potential-energy curves by comparing simulated spectra with actualy observed [18]. Photoassociation

$$\mathrm{Li}(2S) + \mathrm{Zn}(4S) + h\nu \rightarrow \mathrm{LiZn}(2\,^2\Pi) \qquad (2)$$

and bound-bound absorption

$$\mathrm{LiZn}(X^2\Sigma^+) + h\nu \rightarrow \mathrm{LiZn}(2\,^2\Pi) \qquad (3)$$

are two additional paths of the excimer formation as illustrated in Fig. 1 for the LiZn case. According to the results presented in Ref. [11] the photoassociation process (2) can be used to excite higher vibrational levels of the LiZn 2 $^2\Pi$ state, whereas the bound-bound absorption can efficiently populate only the lowest vibrational levels in the 2 $^2\Pi$ state. The advantage of the photoassociation preparation (2) of excimers over the photochemical formation (1) is that the upper-state rovibrational distribution can be calculated assuming the Maxwell-Boltzmann distribution of quasimolecules among continuum states in the ground electronic state $X\,^2\Sigma^+$ (inset in Fig. 1) at a given temperature of the vapor mixture [1].

Considering processes (2) and (3), which were observed in the metal vapor mixtures, one should first provide a sufficient density of heteronuclear collision partners or heteronuclear molecules and second avoid absorption from the homonuclear molecules (mainly alkali-metal dimers) that are always present in the dense mixture. This is, however, not always an easy task. Particularly for the metal vapor mixtures, the first condition implies careful preparation of the metal alloy contained in the heat-pipe ovens. The second condition could be fulfilled with a suitable choice of the laser wavelength for the excitation, narrow laser bandwidth (such as in the LiHg case [17]). In the pulsed laser experiment, appropriate time gating and averaging of the fluorescence signals is necessary.

It is the purpose of this paper to present experimental results and simulations dealing with different aspects for the

*Present address: Institut für Experimentalphysik, Technische Universität Graz, A-8100 Graz, Austria.

 © 1996 The American Physical Society

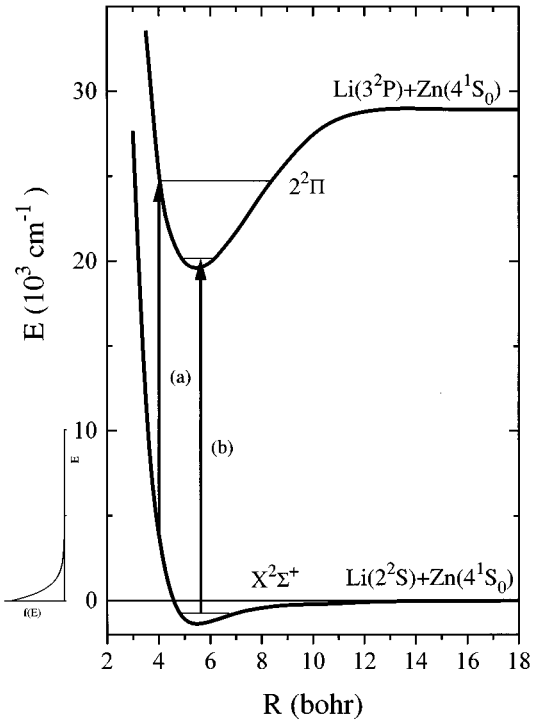

FIG. 1. Illustration of (a) the photoassociation and (b) the bound-bound excitation. $f(E)$ is the Maxwell-Boltzmann distribution of quasimolecules among continuum states in the ground electronic state.

observation of processes (2) and (3) in the alkali-metal–group-II*B* metal vapors. We concentrate on the LiZn, LiCd, and NaZn systems as good test examples.

This paper is organized as follows. Section II presents the theoretical treatment for the processes (2) and (3). Experimental details, including a description of metal alloy preparation, are presented in Sec. III. Experimental results are given in Sec. IV. In Sec. V we discuss the results in comparison with spectral simulations. Finally, conclusions are presented in Sec. VI together with an outlook for future experiments.

II. THEORETICAL TREATMENT

For the photoassociation process, according to Doyle [1] and Sando and Dalgarno [2], the absorption probability per photon can be expressed for Hund's case (a) as

$$k_\nu^{bf}=\frac{1}{Q_T}\frac{8\pi^3\nu}{3hc}n(\mathrm{IA})n(\mathrm{IIB})\times(4\mu/\hbar)\sum_{v'}\sum_{J'}S_{J'J''}\left|\langle b,K_b,J''|D_e(R)|a,v',J'\rangle\right|^2\times\frac{1}{K_b}\exp(-\hbar^2K_b^2/2\mu kT), \tag{4}$$

where $n(\mathrm{I}A)$ and $n(\mathrm{II}B)$ are the number densities of the I*A* and II*B* atoms. $Q_T=(2\pi\mu kT/h^2)^{3/2}$ is the translational partition function for the relative motion. μ is the reduced mass. $K_b=(8\pi^2\mu E_b/h^2)^{1/2}$ is the relative momentum of the colliding pair of atoms. The exponential term is the Maxwell-Boltzmann factor. $h\nu=E_a-E_b$, where E_a is the final-state energy and E_b is the initial-state energy. $S_{J'J''}$ is the Hönl-London factor [19]. $|b,K_b,J''\rangle$ and $|a,v',J'\rangle$ are solutions of the radial Schrödinger equation with the continuum function asymptotically normalized to a unit modulus sine function. $D_e(R)$ is the electronic transition dipole moment function.

For the bound-bound absorption the absorption coefficient can be calculated using [20]

$$\int k_\nu^{bb}d\nu=\frac{8\pi^3\nu}{3hc}\frac{S_{J'J''}}{2J''+1}\left|\langle v',J'|D_e(R)\times|v'',J''\rangle\right|^2N(v'',J''), \tag{5}$$

where $N(v'',J'')$ is the population and $|v'',J''\rangle$ is the wave function of the lower level. The left-hand side of Eq. (5) is evaluated assuming Doppler-broadened molecular line shapes.

The population distribution in the upper excited state following the photoassociation process is

$$P_{v',J'}=\frac{1}{Q_T}n(\mathrm{IA})n(\mathrm{IIB})\sum_{J''}S_{J'J''}\left|\langle b,K_b,J''|D_e(R)\times|a,v',J'\rangle\right|^2\frac{1}{K_b}\exp(-\hbar^2K_b^2/2\mu kT). \tag{6}$$

Once the population distribution in the excited state is known, the resulting bound-free emission spectrum is calculated according to [11,12,20]

$$I_{\mathrm{em}}(\lambda)=\sum_{v'}\sum_{J'}\frac{64\pi^4\nu^6c^2}{3}P_{v',J'}\sum_{J''}S_{J'J''}\left|\langle b,K_b,J''|D_e(R)\times|a,v',J'\rangle\right|^2/K_b. \tag{7}$$

Using Eqs. (4)–(7), the absorption coefficient, the population distribution following the photoassociation process, and the emission spectrum can be simulated.

III. EXPERIMENT

The experimental setup is similar to what is described in Ref. [10]. In brief, a pulsed dye laser (Coumarin 120, range 427–460 nm) pumped by a XeCl excimer laser at 308 nm was used to excite the vapor mixture. The laser energy varied from 0.5 to 3 mJ per pulse and the pulse half-width was about 20 ns with a bandwidth of the laser line about 0.2 cm^{-1}. At typical vapor temperatures of 1000 K the Doppler absorption widths for the LiZn, LiCd, and NaZn molecular transitions are about 0.05 cm^{-1}. Accordingly, the laser can simultaneously excite several rovibrational levels in the LiZn, LiCd, or NaZn $2\,^2\Pi$ states. Fluorescence from the heat pipe oven is dispersed by a 0.6-m scanning monochromator and detected by a photomultiplier (Hamamatsu R2949). The signal was sent to a boxcar averager (PARC M162 and M164) where it was processed and the output was sent to an analog-to-digital converter and an IBM compatible personal computer, where the data were accumulated and analyzed.

Li-Zn and Li-Cd vapor mixtures were produced in a conventional crossed heat-pipe oven. In order to prepare LiZn and LiCd vapor mixtures we mixed Li and Zn (or Cd) in a mole ratio close to 1:1 in the solid phase. The ratio of [Li] and [Zn] in a vapor mixture is then presumably proportional to the ratio of Li and Zn vapor pressures taken from the Nesmeyanov tables [21].

To observe the NaZn excimer emission we need to increase the collision frequency of Na atoms with Zn, which is obtained by putting more Zn than Na atoms in the vapor mixture. In Ref. [15] the [Na] was decreased below the [Zn] by putting Na in boat located at a colder region of the heat-pipe tube. According to the Raoult law [22], we can achieve a similar condition by preparing a NaZn alloy that contains at least 5 times more Zn atoms than Na atoms in the solid phase. To test this assumption we prepared three Na-Zn alloys with mole fraction ratios $x_{\mathrm{Na}}/x_{\mathrm{Zn}}$ equal to 1/2.78, 1/5.67, and 1/16.9 in the solid and liquid phases. The Na-Zn vapor mixture was prepared in another heat-pipe oven with a well-defined column density [23]. The Na-Zn alloy in the horizontal heat-pipe oven was heated by the sodium vapor column in the vertical tube in which the horizontal heat-pipe was argon welded. The diameter of the vertical tube determines the vapor column length in the horizontal heat-pipe oven. In addition, the buffer gas pressure in the vertical tube precisely determines the vapor temperature in the horizontal heat-pipe oven. Such a heat-pipe oven was used for simultaneous measurement of the laser-induced fluorescence and the total absorption coefficient of the Na-Zn vapor mixture. Absorption was measured in an arm of the heat-pipe oven pointing towards the monochromator, using a tungsten halogen lamp. Since the Zn, Zn_2, and NaZn absorption coefficients are negligible (less than 0.05 cm^{-1}) in the visible and near-infrared spectral region, we actually observed only the Na and Na_2 absorption. The Na atom densities were determined from fitting the total absorption coefficient of the Na_2 X-B band [24].

IV. RESULTS

A. Photoassociation

In the region of laser excitation from 460 to 490 nm we can expect the direct bound-bound excitation of intermetallic excimer bands [18]. However, the spectral overlap with alkali-metal dimer X-B absorption preclude its observation. Using the laser wavelengths from 430 to 460 nm, we excite high vibrational levels of the $2\ ^2\Pi$ excimer state, whereby the excitation of the $Li_2\ B^1\Pi_u$ state is avoided. According to our previous spectral simulations of LiZn and LiCd bound-bound and bound-free $2\ ^2\Pi - X^2\Sigma^+$ transitions [11,12], the radiative transitions from these higher excited rovibrational levels are essentially of the bound-free type. In Fig. 2 we present the experimentally observed blue-green bands of LiZn, LiCd, and NaZn molecules, excited by the laser lines at 438.5, 436.5, and 439.5 nm, respectively. The Na-Zn vapor mixture was prepared by introducing a controlled stream of sodium vapor into zinc vapor generated in a conventional crossed heat-pipe oven [15]. Considering the shapes of excimer bands in Fig. 2, which do not show the sharp structures at the band maxima (see Ref. [10] and [14]) stemming from bound-bound contributions, we can conclude that the buffer

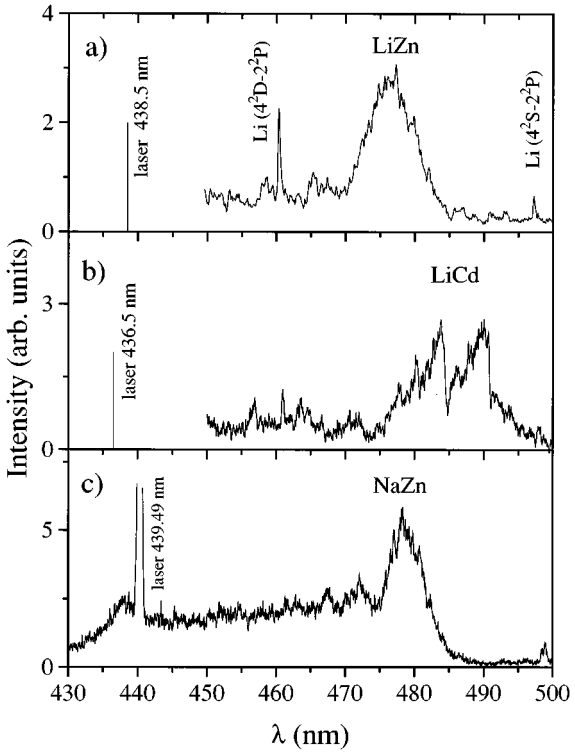

FIG. 2. Spectra of LiZn, LiCd, and NaZn blue-green bands. (a) LiZn-laser wavelength, 438.5 nm; temperature, 1070 K; buffer gas pressure, 50 Torr. (b) LiCd-laser wavelength, 436.5 nm; temperature, 1090 K; buffer gas pressure, 40 Torr. (c) NaZn-laser wavelength, 439.49 nm; temperature, 920 K; buffer gas pressure, 50 Torr.

pressure (up to 50 Torr) is not high enough to enable complete redistribution of the population toward the lowest vibrational levels of the $2\ ^2\Pi$ state in these intermetallic excimers.

We chose the NaZn excimer to study the influence of mole fraction ratio of atoms in the alloy on the outcoming spectrum. Figure 3 shows NaZn spectra measured with Na-Zn alloys, with $x_{\mathrm{Na}}/x_{\mathrm{Zn}}$ equal to 1/2.78, 1/5.67, and 1/16.9 in the solid phase. All three alloys were heated to 840 K and the vapor mixture was excited with the laser line at 440 nm. Figure 3(a) shows the spectrum for $x_{\mathrm{Na}}/x_{\mathrm{Zn}}=1/2.78$. Here we observed the Na_2 diffuse band (free-bound excitation) at 437 nm [25] and collision induced Na_2 interference continuum at 452 nm [26]. The NaZn band at 478 nm as compared to the sodium dimer structures is too weak to be discernible. The absence of NaZn emission in this case additionally indicates that the reaction $Na_2(2\ ^3\Pi_g)$ + Zn is not very efficient in creating the NaZn* excimer. In Fig. 3(b) the mole fraction ratio is $x_{\mathrm{Na}}/x_{\mathrm{Zn}}=1/5.67$ in the Na-Zn alloy and the NaZn band is already discernible in the spectrum. Its shape is slightly different from that in Fig. 2(c), where we have an even higher Zn density in the vapor mixture. In the case of Fig. 3(b) shape has an intensive blue tail in the region from 455 to 470 nm. This blue tail can come partly from the weaker NaZn $3\ ^2\Sigma^+ - X^2\Sigma^+$ transition. The NaZn band looks similar to the spectrum obtained by photochemical excitation, when we prepared the Na_2^* in high rovibrational levels by the excimer laser excitation at 308 nm [15]. In such a case we have the possibility to produce the

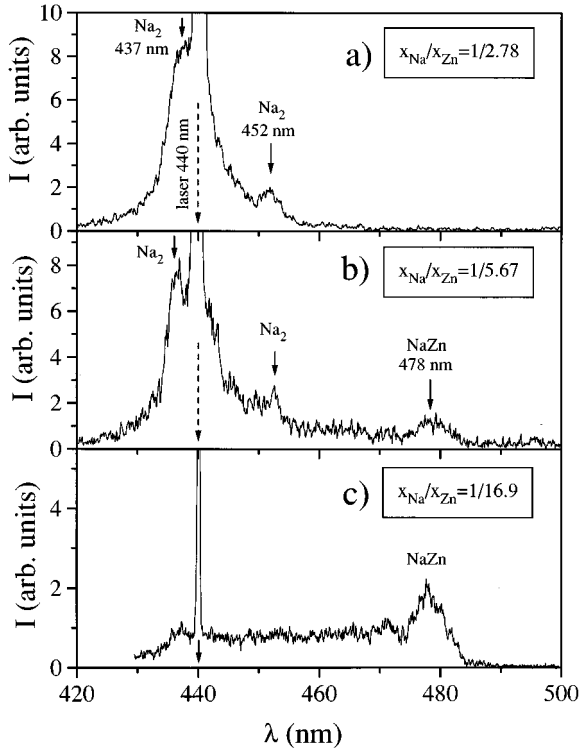

FIG. 3. Spectra of Na-Zn vapor mixture excited by the laser line at 440 nm at the temperature $T=840$ K. The Ar buffer gas pressure was 13.5 Torr in both horizontal and vertical heat-pipe ovens. The Na-Zn alloys were prepared with mole fraction ratios in the solid phase equal to (a) $x_{\mathrm{Na}}/x_{\mathrm{Zn}}=1/2.78$, (b) $x_{\mathrm{Na}}/x_{\mathrm{Zn}}=1/5.67$, and (c) $x_{\mathrm{Na}}/x_{\mathrm{Zn}}=1/16.9$.

NaZn not only in the $2\ ^2\Pi$ state, but also in the $3\ ^2\Sigma^+$ and other neighboring electronic states. In Fig. 3(c) we show the spectrum obtained with the Na-Zn alloy with $x_{\mathrm{Na}}/x_{\mathrm{Zn}}=1/16.9$. The spectrum in Fig. 3(c) looks similar to Fig. 2(c). Note, however, that the laser wavelength is different by 0.5 nm, as compared to Fig. 3(c). The Na_2 structures in Figs. 2(c) and 3(c) are minimized, as compared to Figs. 3(a) and 3(b), because of the low Na_2 density. The NaZn band is observed with a maximum at 478 nm, weak secondary maxima on the short-wavelength side, and a continuum that remain constant in intensity in the range from 435 to 470 nm.

B. Ground-state densities of excimers

In order to see if the ground-state excimer density is large enough for obtaining the bound-bound excitation, we estimated the excimer densities versus temperature from the dissociation equilibrium equation [22]. The dissociation equilibrium equation for the reaction $A+B\rightarrow AB$ is given by

$$[AB]=3.292\times10^{-29}\frac{g_{AB}}{g_A g_B}\sqrt{\left(\frac{m_{AB}}{m_A m_B}\right)^3}\frac{\sqrt{T}}{\sigma B_e}\times\frac{e^{1.4388D_e/T}}{1-e^{-1.4388\omega_e/T}}[A][B], \tag{8}$$

where $[AB]$, $[A]$, and $[B]$ are the densities in m^{-3}. T is the temperature in K. D_e is the dissociation energy and ω_e and

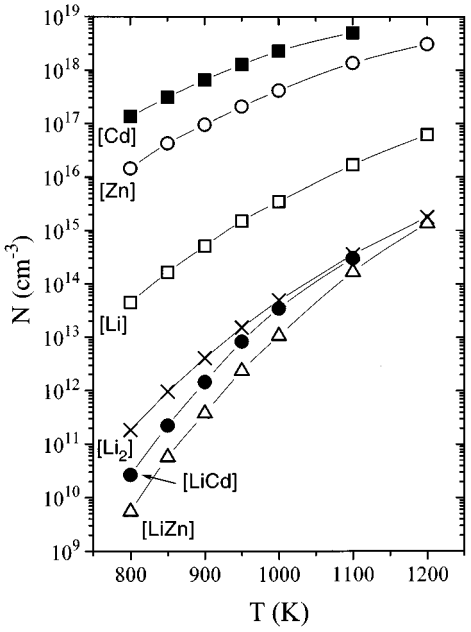

FIG. 4. [Li], [Zn], [Cd], [Li_2], [LiZn], and [LiCd] densities versus temperature. [Li], [Zn], [Cd], and [Li_2] are taken from the Nesmeyanov tables. Raoult's law is applied for x_{Li}: $x_{\mathrm{Zn(Cd)}}=0.5{:}0.5$. [LiZn] and [LiCd] are estimated using the equation of the dissociation equilibrium (8) for the reactions LiZn→Li+Zn and LiCd→Li+Cd, respectively.

B_e are vibrational and rotational molecular constants, respectively, of the ground state AB molecule in cm^{-1}. σ is a symmetry factor, which is equal to 1 for the heteronuclear and equal to 2 for the homonuclear molecule. m_{AB}, m_A, and m_B are molar masses in g/mol. g_{AB}, g_A, and g_B are the statistical weights of the ground molecular and atomic states. Figure 4 presents the densities of Li, Zn, Cd, Li_2, LiZn, and LiCd. Li and Zn (Cd) atom densities are calculated from the values given in the Nesmeyanov tables multiplied by the mole fractions $x_{\mathrm{Li}}=x_{\mathrm{Zn(Cd)}}=0.5$, according to the Raoult's law. The Li_2 density from the Nesmeyanov tables were multiplied by x_{Li}^2. The LiZn density calculated from Eq. 8, with ground-state spectroscopic constants published in [10], is about one order of magnitude smaller than the Li_2 density, but still large enough for obtaining the bound-bound excitation. The LiCd density is even higher and approaches the Li_2 density at temperatures larger than 1000 K. We calculated the Na, Zn, Na_2, and NaZn densities versus temperature using Eq. (8), which are shown in Fig. 5 for all three above-mentioned Na-Zn alloys. The Na and Zn atom densities are taken from the Nesmeyanov tables and multiplied with the corresponding mole fractions for Na and Zn. The density, which corresponds to the spectrum in Fig. 3(a), can be obtained from Fig. 5(a). The Na and Zn densities are almost the same, but the Na_2 density is about two orders of magnitude higher than NaZn density. In Fig. 5(b), which corresponds to the spectrum in Fig. 3(b), the Zn density is slightly higher than the Na density. The NaZn density is not much different from those in Fig. 5(a), but the Na_2 density is almost one order of magnitude smaller than in Fig. 5(a). In Fig. 5(c), which describes the situation in the vapor mixture as in Fig. 3(c), the Zn density is one order of magnitude

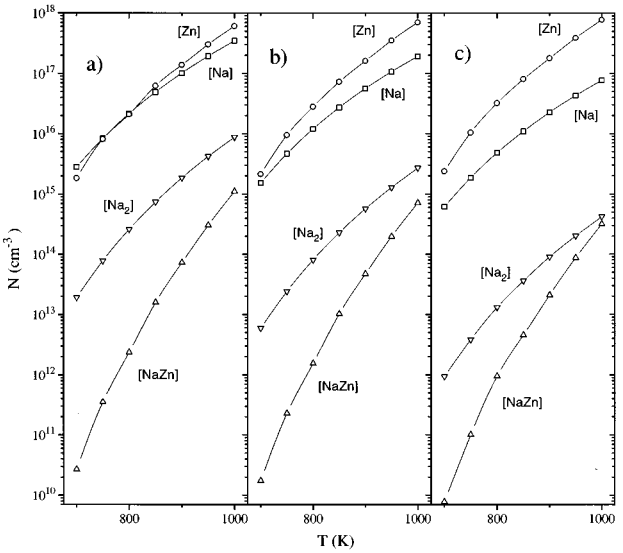

FIG. 5. [Na], [Zn], [Na_2], and [NaZn] densities versus temperature for three Na-Zn alloys, prepared with mole fraction ratios in the solid phase equal to (a) $x_{Na}/x_{Zn}=1/2.78$, (b) $x_{Na}/x_{Zn}=1/5.67$, and (c) $x_{Na}/x_{Zn}=1/16.9$.

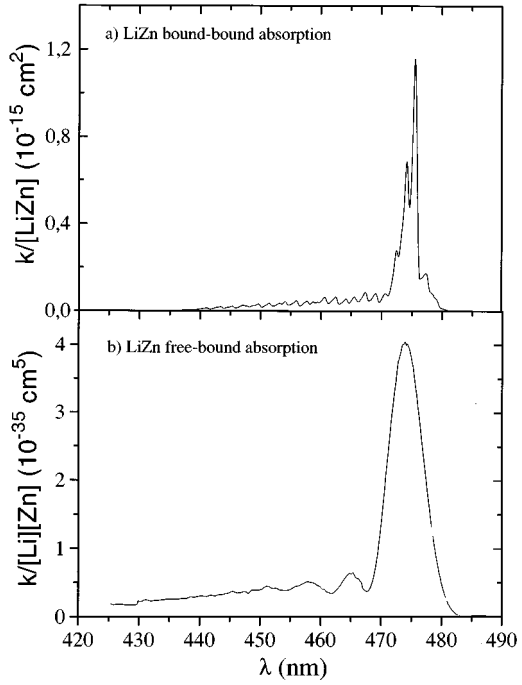

FIG. 6. Calculated absorption coefficients for LiZn: (a) bound → bound absorption and (b) free→bound absorption. $T=1000$ K.

higher than the Na density at a given temperature range. Now the NaZn and Na_2 densities approach each other at higher temperatures and the possibility for the direct excitation of the NaZn increases, as compared to the Na_2 X-B excitation. Table I gives a comparison of estimated (from Raoult's law) and experimental values of sodium atom densities at 840 K. These two sets of values differ by about 30%.

V. SPECTRAL SIMULATIONS AND DISCUSSION

We have chosen the LiZn for the further detailed spectral analysis as it is the simplest among alkali-metal–group-IIB systems [11,12]. Spectral simulations of the blue-green band were performed using the potential-energy curves and the transition dipole moment function published in our previous paper [10].

We first calculated the reduced free-bound and the bound-bound absorption coefficients in order to see which process is more probable for the laser excitation in the region of 435–450 nm. In the simulation of the absorption coefficient for the photoassociation process the free-bound type overlap integrals $|\langle b,K_b,J''|D_e(R)|a,v',J'\rangle|^2$ of the LiZn $2\,^2\Pi\rightarrow X^2\Sigma^+$ transition for $v'=0-40$, $J'=0.5-150.5$ were calculated. The reduced absorption coefficient k/[Li][Zn] was calculated in the next step for the whole spectral range of the blue-green band. For the bound-bound contribution to the absorption coefficient the overlap integrals $|\langle v',J'|D_e(R)|v'',J''\rangle|^2$ were calculated for all bound rovibrational levels in the LiZn ground state. The bound-bound transitions to higher ($v'>10$) rovibrational levels of the $2\,^2\Pi$ state are of negligible intensity. The reduced bound-bound absorption coefficient k/[LiZn] was calculated at temperature $T=1000$ K. The absorption cross sections for the free-bound and bound-bound transitions are separately shown in Figs. 6(a) and 6(b), respectively. To obtain relevant absorption coefficients and compare free-bound and bound-bound contributions, we used estimates of the atomic and molecular densities presented in Sec. IV. Both the bound-bound and the free-bound excitations are comparable over a narrow spectral region around 470–480 nm. The bound-bound absorption coefficient decreases rapidly with decreasing wavelength. As the calculated ground-state potential-energy curves are expected to be too deep, the reduced bound-bound absorption coefficient should be even lower than free-bound absorption in the region of our laser excitation. In addition, too large value of the LiZn ground-state spectroscopic constant $D_0=1250$ cm^{-1} [10] can cause the overestimation of the LiZn density at 1000 K by a factor of 2. The expected value of the ground state D_0 for the LiZn should be about 900 cm^{-1}, as compared to the LiCd [14] and LiHg [17] cases. All this leads to the conclusion that the spectra observed in Figs. 2 and 3 are excited in the photoas-

TABLE I. Sodium atomic densities for different Na-Zn alloys obtained experimentally and estimated by using Raoult's law. The x_{Na}/x_{Zn} is the mole fraction ratio in the solid phase.

x_{Na}/x_{Zn}	[Na] Expt. (cm^{-3})	[Na] Theor. (cm^{-3})
1/2.78	4.1×10^{16}	4.5×10^{16}
1/5.67	3.6×10^{16}	2.5×10^{16}
1/16.9	1.5×10^{16}	9.6×10^{15}

TABLE II. R_e and D_e values for the ground-state LiZn, LiCd, LiHg, NaZn, NaCd, NaHg, KZn, KCd, and KHg molecules from *ab inito* and model potential-energy curve calculations, scattering, and laser-induced fluorescence experiments.

Molecule	R_e (bohrs)	D_e (cm^{-1})	Reference
LiZn	5.53	1314	*ab initio* [10]
LiCd	5.7	1426	*ab initio* [14]
LiHg		789 ± 32	fluorescence [27]
	5.73	645	*ab initio* [28]
	5.67	851	scattering [29]
	5.71	856	model potential [30]
NaZn	6.45	830	*ab inito* [15]
NaCd	6.3	481	*ab inito* [31]
NaHg	6.5	593	model potential [32]
	6.4	1208	*ab inito* [33]
	8.9	443	scattering [34]
KZn	8.2	232	model potential [35]
KCd	8.0	300	model potential [35]
KHg	7.4	520	model potential [35]
	9.3	423	scattering [36]

sociation process. Since the LiCd excimer band maxima at 483 and 490 nm are separated from the laser excitation wavelength more than in the case of LiZn and NaZn (see Fig. 2), the LiCd seems to be a good candidate for the observation of the photoassociation process. NaZn is also a good candidate for the photoassociation process because its ground state is shallower than Li-II*B* ground states. Table II gives available R_e and D_0 values for the ground states of alkali-metal–group-II*B* molecules. Although most of the values are theoretical, with insufficient accuracy, general trends are visible.

We provided the spectral simulation of the LiZn $2\,^2\Pi - X^2\Sigma^+$ transition, assuming the free-bound excitation of the $2\,^2\Pi$ state, as described in the procedure from Sec. II. Because of the large number of excited-state rovibrational levels that are excited by photoassociation a large number of different structured continua are superimposed and the individual structure is almost entirely smeared out. The calculated population distribution for the effective temperature at 1000 K and the laser excitation at 438.5 nm is shown in Fig. 7. The rovibrational distribution is rather broad with most probable $(v'J')$ around (8–10, 100). Figures 8(a) and 8(b) show the comparison of the experimental and simulated LiZn spectra for the laser excitation at 438.5 nm. The enhancement of the calculated fluorescence intensity around

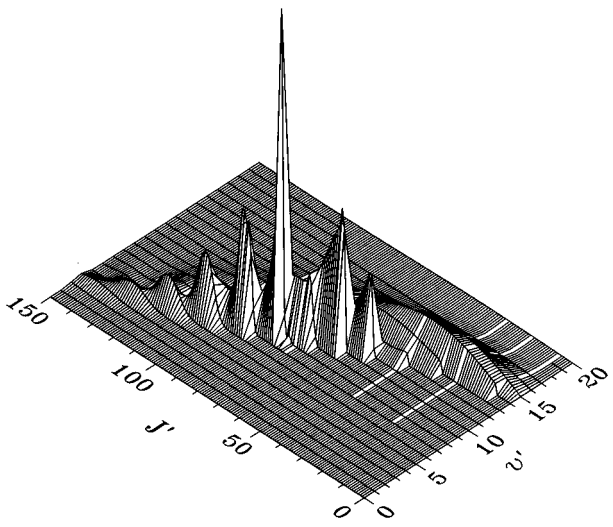

FIG. 7. Simulated population distribution for LiZn($^2\Pi$) at $T=1000$ K upon laser excitation at $\lambda = 438.5$ nm.

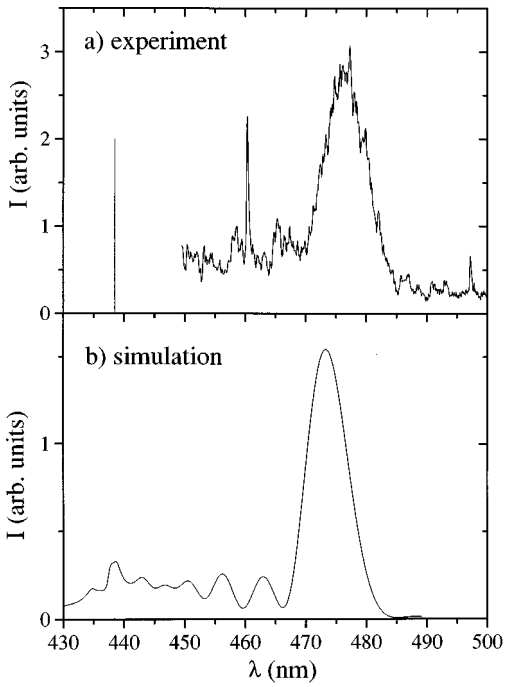

FIG. 8. Comparison of (a) experimentally observed and (b) simulated LiZn blue-green bands. The temperature in the experiment was $T=1070$ K and the buffer gas pressure was 50 Torr. The calculated population distribution is given in Fig. 7.

the laser line in Fig. 8(b) could be attributed to selective absorption, where only free-bound transitions with large absorption probability are excited to the upper state. The shift of the calculated and observed band peak of about 4 nm is attributed to insufficient accuracy in determining the relevant difference potential [10]. Relatively good agreement between observed and simulated LiZn band shapes shows that the LiZn 2 $^2\Pi$ state is excited in the photoassociation process.

VI. CONCLUSIONS

We have observed LiZn, LiCd, and NaZn 2 $^2\Pi \rightarrow 1\,^2\Sigma^+$ emission, where the 2 $^2\Pi$ states were excited by laser wavelengths between 435 and 450 nm. The analysis of spectral shapes indicates that the free-bound excitation is dominant. This is supported by calculation of bound-bound and free-bound absorption coefficients. Simulation of the LiZn 2 $^2\Pi - X^2\Sigma^+$ transition, with the upper-state population distribution achieved by free-bound laser excitation at 438.5 nm, shows satisfactory agreement with the experimental spectrum.

We have shown that specific choice of alloys and use of advanced heat-pipe ovens, in addition to suitable laser excitation, provides the necessary basis for laser-induced fluorescence studies of intermetallic molecules. The remaining problem of spectrally resolving the alkali-metal–group-II*B* bands from the alkali-metal dimer bands can be solved by using time-resolved spectroscopy with a subnanosecond pulsed laser, because the radiative depopulation of the excited alkali-metal dimer is usually faster. Such experiments are proposed for future investigation of the I*A*-II*B* excimers.

ACKNOWLEDGMENTS

This work was financially supported by the Ministry of Science of the Republic of Croatia. We gratefully acknowledge partial support from the Humbolt Stiftung and from the partnership project of the Volkswagenwerk Stiftung, Germany.

[1] R. O. Doyle, J. Quant. Spectrosc. Radiat. Transfer **8**, 1555 (1968).
[2] K. M. Sando and A. Dalgarno, Mol. Phys. **20**, 103 (1971).
[3] P. S. Herman and K. M. Sando, J. Chem. Phys. **68**, 1153 (1978).
[4] W. T. Luh, K. M. Sando, A. M. Lyyra, and W. C. Stwalley, Chem. Phys. Lett. **144**, 221 (1988).
[5] H. Scheingraber and C. R. Vidal, J. Chem. Phys. **66**, 3694 (1977).
[6] G. Rodriguez and J. G. Eden, J. Chem. Phys. **95**, 5539 (1991).
[7] L. P. Ratliff, M. E. Wagshul, P. D. Lett, S. L. Rolston, and W. D. Philips, J. Chem. Phys. **101**, 2638 (1994).
[8] C. J. Williams and P. S. Julienne, J. Chem. Phys. **101**, 2634 (1994).
[9] R. A. Cline, J. D. Miller, and D. J. Heinzen, Phys. Rev. Lett. **73**, 632 (1994).
[10] S. Milošević, X. Li, D. Azinović, G. Pichler, M. C. van Hemert, and R. Düren, J. Chem. Phys. **96**, 7364 (1992).
[11] X. Li, S. Milošević, D. Azinović, G. Pichler, R. Düren, and M. C. van Hemert, Z. Phys. D **30**, 39 (1994).
[12] X. Li, Ph.D thesis, Institute of Physics, University of Zagreb, 1992 (unpublished).
[13] R. Düren, B. Heuman, and S. Milošević, Max-Planck-Institute für Strömungsforschung, Göttingen, Report No. 14, 1994 (unpublished).
[14] M. C. van Hemert, D. Azinović, X. Li, S. Milošević, G. Pichler, and R. Düren, Chem. Phys. Lett. **200**, 97 (1992).
[15] D. Azinović, X. Li, S. Milošević, G. Pichler, M. C. van Hemert, and R. Düren, J. Chem. Phys. **98**, 4672 (1993).
[16] D. Azinović, Ph.D thesis, Institute of Physics, University of Zagreb, 1994 (unpublished).
[17] D. Gruber, X. Li, L. Windholz, M. M. Gleichmann, B. A. Heß, I. Vezmar, and G. Pichler (unpublished).
[18] S. Milošević, in *Spectral Line Shapes*, edited by A. D. May *et al.*, AIP Conf. Proc. No. 328 (AIP, New York, 1995), pp. 391–405.
[19] G. Herzberg, *Spectra of Diatomic Molecules* (Van Nostrand, Princeton, 1950).
[20] J. Tellinghuisen, in *Photodissociation and Photoionization*, edited by K. P. Lawley, Advances in Chemical Physics Vol. LX (Wiley, New York, 1985), p. 299.
[21] A. N. Nesmeyanov, in *Vapor Pressure of the Chemical Elements*, edited by R. Gray (Elsevier, New York, 1963).
[22] P. W. Atkins, *Physical Chemistry* (Oxford University Press, Oxford, 1993), pp. 162 and 608.
[23] H. Scheingraber and C. R. Vidal, Rev. Sci. Instrum. **52**, 1010 (1981).
[24] R. E. M. Hedges, D. L. Drummond, and A. Gallagher, Phys. Rev. A **6**, 1519 (1972).
[25] G. Pichler, S. Milošević, D. Veža, and R. Beuc, J. Phys. B **16**, 4619 (1983).
[26] G. Pichler, J. T. Bahns, K. M. Sando, W. C. Stwalley, D. D. Konowalow, L. Li, R. W. Field, and W. Müller, Chem. Phys. Lett. **129**, 425 (1986).
[27] D. Gruber and X. Li, Chem. Phys. Lett. **240**, 42 (1995).
[28] M. Gleichmann and B. A. Hess, J. Chem. Phys. **101**, 9691 (1994).
[29] U. Buck, H. O. Hope, F. Huisken, and H. Pauly, J. Chem. Phys. **60**, 4925 (1974).
[30] R. E. Olson, J. Chem. Phys. **49**, 4499 (1968).
[31] C. Angeli, M. Persico, M. Allegrini, G. De Filippo, F. Fuso, D. Gruber, L. Windholz, and M. Musso, J. Chem. Phys. **102**, 7782 (1995).
[32] E. Czuchaj, F. Rebentrost, H. Stoll, and H. Preuss, Chem. Phys. Lett. **187**, 246 (1991).
[33] L. Windholz, G. Zerza, G. Pichler, and B. Hess, Z. Phys. D **18**, 373 (1991).
[34] L. Hüwel, J. Maier, and H. Pauly, J. Chem. Phys. **76**, 4961 (1982).
[35] E. Czuchaj, F. Rebentrost, H. Stoll, and H. Preuss, Chem. Phys. Lett. **218**, 454 (1994).
[36] U. Lackschewitz, J. Maier, and H. Pauly, J. Chem. Phys. **84**, 181 (1986).